

SEEDING HYDRATE FORMATION IN WATER-SATURATED SAND WITH DISSOLVED-PHASE METHANE OBTAINED FROM HYDRATE DISSOLUTION: A PROGRESS REPORT

W.F. Waite^{1*}, J.P. Osegovic², W.J. Winters¹, M.D. Max², D.H. Mason¹

¹U.S. Geological Survey
384 Woods Hole Road
Woods Hole, MA 02543
USA

²Marine Desalinization Systems
1601 3rd St. South
St. Petersburg, FL 33701
USA

ABSTRACT

An isobaric flow loop added to the Gas Hydrate And Sediment Test Laboratory Instrument (GHASTLI) is being investigated as a means of rapidly forming methane hydrate in water-saturated sand from methane dissolved in water. Water circulates through a relatively warm source chamber, dissolving granular methane hydrate that was pre-made from seed ice, then enters a colder hydrate growth chamber where hydrate can precipitate in a water-saturated sand pack. Hydrate dissolution in the source chamber imparts a known methane concentration to the circulating water, and hydrate particles from the source chamber entrained in the circulating water can become nucleation sites to hasten the onset of hydrate formation in the growth chamber. Initial results suggest hydrate grows rapidly near the growth chamber inlet. Techniques for establishing homogeneous hydrate formation throughout the sand pack are being developed.

Keywords: gas hydrates, methane, dissolved-phase, solubility

NOMENCLATURE

A : cross-sectional area of the sample [cm^2]
 k : permeability [cm^2/s]
 k_0 : initial permeability [cm^2/s]
 L : sample length [cm]
 M : moles of methane per cubic centimeter [mol/cc]
 ΔP : pressure difference across the sample [MPa]
 Q : fluid flow rate through the sample [cc/min]
 Q_0 : initial fluid flow rate through the sample [cc/min]
Subscripts: *Interface* (*Interface Chamber*), *Source* (*Source Chamber*), *Growth* (*Growth Chamber*), *G* (*gas*), *H* (*hydrate*), *IW* (*initial, pre-dissociation water*), *FW* (*final, post-dissociation water*) [unitless]
 T : temperature [$^{\circ}\text{C}$]
 V : volume in cubic centimeters [cc]

μ : dynamic viscosity of the fluid [$\text{Pa}\cdot\text{s}$]
 ϕ : porosity in hydrate-bearing sediment [unitless]
 ϕ_0 : porosity in hydrate-bearing sediment [unitless]

1. INTRODUCTION

Formation of naturally-occurring gas hydrate, which is most commonly methane hydrate [1], alters sediment properties when the crystalline solid replaces pore water [2, 3]. How sediment properties change depends on where hydrate forms within the pore space, which in turn depends on the formation environment. For example, in partially water-saturated, gas-rich environments, hydrate tends to cement sediment grains together, and even a small amount of hydrate significantly increases seismic wave speeds [4, 5]. In contrast, hydrate formed in water-saturated systems from

* Corresponding author: Phone: +1 508 457 2346 Fax +1 508 457 2310 E-mail: wwaite@usgs.gov

gas dissolved in pore water does not preferentially grow at grain contacts [6]. Relative to cementation, hydrate formation away from grain contacts generates only a limited wave speed increase until the pore-space hydrate saturation exceeds 40-50% [7, 8]. Because many naturally-occurring hydrate reservoirs are thought to form in the absence of free gas [9], testing models relating pore-space hydrate saturation to seismic wave speed requires samples formed from dissolved-phase methane.

Using a glass bead pack, Spangenberg et al. [10] saturated ~95% of the pore space with hydrate formed from dissolved-phase methane in ~50 days by circulating water via an interface chamber in which water dripped through methane gas. We seek to accelerate the growth rate and reduce the time required for each experiment by adding a hydrate source chamber to the system described by Spangenberg et al. [10].

The mechanical properties of hydrate-bearing sediment depend on the extent to which hydrate binds sediment grains together [11, 12], so a concern with accelerated hydrate growth is the shape of the hydrate crystal and the resulting contact between hydrate and sediment grains. As the growth rate for hydrate increases, crystals form in a more dendritic pattern [13, 14]. When the growth rate is slow, hydrate forms faceted crystals and binds more strongly to the sediment particles [14]. The faceted crystal growth morphology can also be attained by annealing rapid-growth hydrate at conditions near the hydrate phase boundary [15] however, so the primary goal in this work was to develop a technique to form hydrate relatively rapidly utilizing methane dissolved in water.

We have configured the Gas Hydrate And Sediment Test Laboratory Instrument (GHASTLI) [2] as a flow loop. Water leaving a methane gas/water interface chamber passes through a source chamber containing granular methane hydrate, pre-made from seed ice, before entering water-saturated sand in a growth chamber. Circulating water dissolves hydrate in the source chamber, acquiring a well-constrained methane saturation, as well as entraining hydrate micro-crystals sloughed off the source-chamber hydrate. In the presence of the hydrate crystals, water entering the relatively cool growth chamber becomes supersaturated with respect to methane as it cools. Methane in excess of the solubility limit can precipitate as hydrate, using the hydrate micro-crystals as nucleation sites. We describe this tech-

nique here, and present results from two preliminary tests.

2. APPARATUS

The flow loop consists of three distinct subsystems designed to control the methane saturation and maintain a bubble-free growth chamber (Fig. 1): 1) a room-temperature methane gas/water interface chamber and a constant flow-rate circulating pump, 2) a temperature-controlled methane hydrate source chamber, and 3) a temperature-controlled, water-saturated sand sample in a hydrate growth chamber.

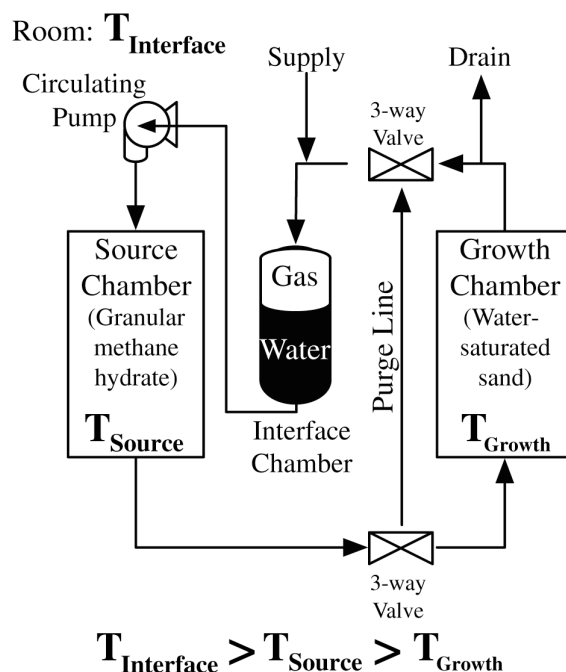


Figure 1: Flow loop schematic. Warm, methane-rich water is pumped from the methane interface chamber to the cooler source chamber, where it passes through a porous network of granular methane hydrate pre-made from seed ice. Hydrate dissolution raises the water’s methane content to the equilibrium solubility at a temperature T_{Source} , which exceeds the equilibrium solubility in the presence of hydrate for the water-saturated sand held in the growth chamber at T_{Growth} . Water entering the sand pack is therefore supersaturated in methane, acting as a methane source for additional hydrate formation.

2.1. Interface chamber and circulating pump:

This subsystem is the gas-phase methane reservoir, which imparts a preliminary degree of methane

saturation to the circulating water while storing gas purged from the rest of the apparatus. Initially, the flow loop is brought to its operating pressure of 12 MPa using pressurized methane gas introduced through the flow loop "supply" inlet (Fig. 1).

A Quizix-brand QL-6000 dual-piston pump delivers water at a constant, user-defined flow rate as described in the procedure. Once flow through the complete system begins, methane-depleted water returning from the growth chamber enters the top of the interface chamber, partially resaturating with methane as it drips through free methane gas. A custom-designed float rests on the gas-water interface, monitored via a Schaevitz-brand magnetic sensor to track free gas consumption. Pressure is monitored using a pressure sensor located at the top of the interface chamber. Temperature is measured by a thermistor held against the chamber's outer wall. A lamp warms the interface chamber's downstream end, reducing the methane concentration in the circulating water below the source vessel's equilibrium methane solubility in the presence of hydrate (See "Interface" and

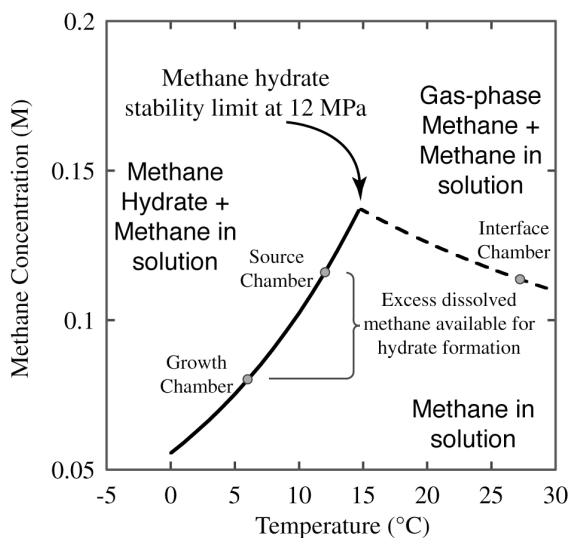


Figure 2: Methane solubility at 12 MPa for individual system components (circles), plotted on the equilibrium solubility curve for methane hydrate and water (solid curve), or methane gas and water (dashed curve). Equilibrium curves are calculated from the online models by Duan [27, 30]. The interface chamber must be held at a temperature high enough to keep the solubility below that of the source chamber, or hydrate will form, rather than dissolve, in the source chamber and clog the flow loop.

"Source Chamber" circles in Fig. 2).

2.2. Source chamber:

Pure, granular methane hydrate is formed in the source chamber in a separate, high-pressure system prior to being connected to the flow loop. Initially, water ice is mixed with a small amount of liquid nitrogen, ground with a mortar and pestle, then sieved to obtain the 180-250 μm grain size fraction. Following the method of Stern et al. [16, 17], methane hydrate is formed by warming the granular water ice in a pressurized methane atmosphere from -20 to $+17^\circ\text{C}$ over the course of 17 hours. The sample is held at 17°C for 24 hours before being reduced to 6°C in preparation for transfer into the flow loop. Once hydrate formation is complete, the source chamber contains a porous network of methane hydrate grains, with methane gas-filled pore space.

The chamber is transferred, under pressure and at 6°C , to a temperature-controlled bath and connected to the flow loop system. To purge free gas from the granular methane hydrate, water is pumped backward through the source chamber (from bottom to top) and into the interface chamber (Fig. 1). Flow continues through the purge line until gas no longer enters the interface chamber, as indicated by stabilization of the interface chamber float position. During flow-loop circulation, water is pumped through the source chamber from top to bottom to ensure residual gas-phase methane remains in the source chamber rather than being transported to the growth chamber. Temperature is measured via two internal thermocouples, one near each end of the chamber. Pressure is monitored with sensors in the flow line between the interface and source chambers, and between the source and growth chambers.

Methane hydrate dissolution in the source chamber not only provides a means of imparting a well-constrained methane saturation level to the circulating water that is nearly independent of pressure [18], but can also slough off hydrate particles which can then nucleate hydrate formation in the growth chamber [13]. Given the 1-5 cc/min flow rates, the chamber geometry and exposed hydrate surface area in the source chamber, water leaving the source vessel would be fully saturated with methane even if the methane hydrate dissolution rate in fresh water were nearly twelve orders of magnitude slower than the $0.4 \text{ mmol CH}_4/\text{m}^2\cdot\text{s}$ rate determined by Rehder et al. [19] in experiments conducted in Monterey Bay.

2.3. Growth chamber:

Growth chamber characteristics and measurement capabilities are described in detail by Winters et al. [2]. The growth chamber contains a water-saturated, Ottawa sand with a 0.25 to 0.5-mm grain size range. The cylindrical sample (nominal length: 134 mm, diameter: 72 mm) is jacketed in a 0.65-mm-thick Viton membrane and capped at both ends with titanium endcaps. The endcaps house transducers for measuring acoustic wave speeds along the sample's long axis. Circulating water enters (or exits) the sample through annular diffuser plates in each endcap.

Confining and pore pressures are maintained independently by Isco-brand 500D syringe pumps. Pressures are measured using sensors located in the flow and chamber pressurization lines outside the growth chamber.

Temperature is maintained using an external bath pumping ethylene glycol through cooling coils surrounding the chamber and through a heat exchanger held against the sample's top endcap. Temperature is monitored with four thermocouples and four thermistors within the chamber, held against the sample sides and spaced to cover the full length of the sample. Each endcap has an embedded thermocouple.

3. PROCEDURE

A flow-loop test consists of three phases: 1) pressurization, 2) hydrate growth, and 3) dissociation.

3.1. Pressurization:

The three flow-loop subsystems are initially pressurized independently. The hydrate source chamber is connected under pressure, and the system is then pressure-equilibrated. The flow loop and pore pressure are increased to 12 MPa by feeding methane through the supply line near the top of the interface chamber (Fig. 1). The confining pressure is raised to 12.25 MPa using an Isco-brand 500D syringe pump to impart a 0.25 MPa effective stress on the water-saturated sand in the growth chamber. In addition to simulating the confining load on buried sediment, the effective pressure holds the sample jacket against the sample, forcing flow to pass through, rather than around, the sand pack.

3.2. Hydrate growth:

Hydrate formation and growth are regulated by manipulating methane solubility with temperature

[13]. Two hydrate formation techniques have been tested: 1) continuous flow, with a constant temperature difference between the source and growth chamber, and 2) episodic flow with a temperature cycle between flow intervals.

In the continuous-flow case, the source chamber is held at 12°C, which, at 12 MPa, is within the hydrate stability field and near the peak of the solubility curve shown in Fig. 2. This temperature was chosen to maximize the quantity of methane transported to the sand sample, held at 6°C, while maintaining nearly a 3°C temperature window for fluid to warm during transport to the growth chamber without producing methane bubbles. Water exiting the interface chamber must be heated above 25°C to ensure that it is undersaturated with methane relative to water in the source chamber (Fig. 2). This requirement forces water entering the source chamber to dissolve, rather than form, methane hydrate. Circulating water entering the growth vessel is cooled relative to the source vessel, and in the presence of hydrate, this cooling produces a state of methane supersaturation in the water entering the growth chamber.

The flow rate is initially set to 5 cc/min, then manually reduced over time as the sample permeability decreases and the pressure required to maintain flow increases. Flow cannot be driven by pressures exceeding the 12.25 MPa confining pressure in the growth chamber, or circulating water would be able to expand the Viton jacket and flow around, rather than through, the sand sample. The hydrate formation phase ends when a 1 cc/min flow rate can no longer be maintained.

For the episodic flow case, the source chamber is still held at 12°C and 12 MPa. During periods of flow, however, the growth chamber is held at 10°C, while a minimum of 1800 cc of methane-rich water is pumped through the sample for ~6 hours at 5 cc/min. This volume is ten times the sample's total pore space. Between periods of flow, the growth chamber is cooled to 6°C to increase the methane supersaturation and thus the amount of methane available for hydrate formation. The system is allowed to equilibrate for ~43 hours before rewarming to 10°C and repeating the cycle. In the test described here, six flow cycles were completed.

3.3. Hydrate dissociation:

With the inlet and outlet flow lines closed, the growth chamber temperature is raised to 20°C at

.66 °C/hour, dissociating any hydrate in the growth chamber. The total amount of hydrate contained in the growth chamber is estimated from the methane solubility and the observed pore pressure response during dissociation, as discussed below.

4. RESULTS AND DISCUSSION

4.1. Continuous flow test:

Open circles in figure 3 show the pore pressure increase in the growth chamber in response to warming the sample through the hydrate stability temperature (diamonds and solid curve, data combined from Jhaveri and Robinson [20], deRoo et al. [21], Yang et al. [22]). The initial pore pressure is slightly below 8.4 MPa because of a shear strength test performed prior to dissociation. Axial deformation of the sample during shear causes the pore space to dilate, reducing the pressure from 12 to ~8.4 MPa. Temperature measurements are made on the outer sample surface, meaning the sample interior is slightly cooler, particularly during the period of active dissociation. The pressure increase along the methane hydrate equilibrium curve indicates methane hydrate is breaking down, increasing pressure as free gas forms from dissociating hydrate. Once hydrate is consumed, a portion of the free gas produced goes into solution,

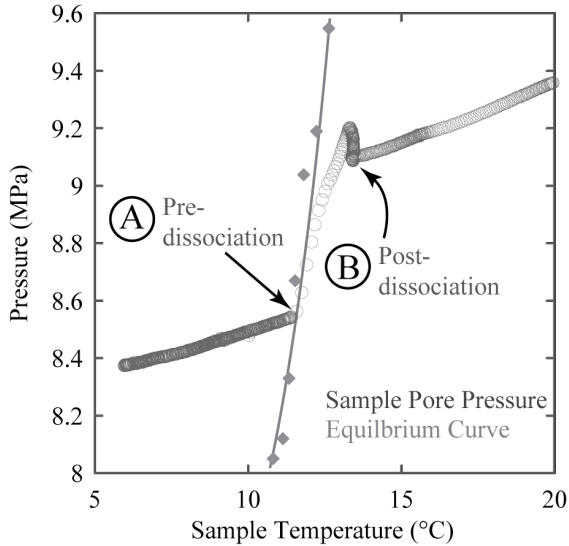


Figure 3: Pore pressure versus temperature during hydrate dissociation in the growth chamber. Tracking of the measured pressure and temperature (circles) along the hydrate equilibrium curve (diamonds and solid curve, from Jhaveri and Robinson [20], deRoo et al. [21], Yang et al. [22]) indicates hydrate has formed in the growth chamber.

lowering the measured pore pressure to 9.09 MPa from its peak of ~9.2 MPa.

To calculate the hydrate volume, the sealed growth chamber is assumed to contain a constant number of methane molecules before and after dissociation. Prior to dissociation, the pore space is assumed to contain only methane hydrate and water, with free methane gas and methane-saturated water being the only post-dissociation pore constituents. The methane budget can be cast in terms of moles of methane per cc in each phase, M , and the volume of each phase, V as:

$$M_H \cdot V_H + M_{IW} \cdot V_{IW} = M_G \cdot V_G + M_{FW} \cdot V_{FW}, \quad (1)$$

where the subscripts H and G refer to hydrate and gas, while IW and FW refer to the initial, pre-dissociation water volume, and the final, post-dissociation water volume, respectively.

When hydrate dissociates, the water volume produced can be related to the original water volume using the density of water molecules in the hydrate phase compared to the density of liquid water. At pre-dissociation conditions of 8.55 MPa and 11.6°C, point "A" in Fig. 3, the methane hydrate unit cell volume given by Shpakov et al. [23] is 1.71×10^{-21} cc, meaning the hydrate density considering water molecules alone is 0.804 g/cc. Following dissociation, the water density at 9.09 MPa and 13.4°C, is 0.99958 g/cc [24], point "B" in Fig. 3. Relative to the initial hydrate volume, V_H , the initially hydrate-bound water occupies a volume $V_H \cdot (0.804 \text{ g/cc}) / (0.99958 \text{ g/cc}) = 0.805 \cdot V_H$ after dissociation. Gas takes up the remaining portion of the volume previously occupied by hydrate: $V_G = 0.195 \cdot V_H$. For one cubic centimeter of pore space, Eq. 1 volumes can be related to the initial hydrate volume through:

$$V_{IW} = 1 - V_H, \quad (2a)$$

$$V_{FW} = V_{IW} + 0.805 \cdot V_H, \quad (2b)$$

$$V_G = 0.195 \cdot V_H. \quad (2c)$$

The number of moles of methane per cc, M , must be calculated for each phase:

Hydrate: In methane hydrate, a non-stoichiometric material in which the ratio of methane to water molecules varies, we assume a constant ratio of 6 water molecules per methane molecule, found by Circone et al. [25] to be representative of methane hydrate held near its phase boundary. Combining this ratio with the unit cell volume measured by

Shpakov et al. [23] for point "A" in Fig. 3, yields $M_H = 7.4 \times 10^{-3}$ moles of methane per cc of hydrate.

Gas: For post-dissociation conditions of 9.09 MPa and 13.4°C, point "B" in Fig. 3, the methane density is 4.6×10^{-3} moles of methane per cc gas [26, 27].

Water: Prior to dissociation at 8.55 MPa and 11.6°C, point "A" in Fig. 3, $M_{IW} = 8.17 \times 10^{-5}$ moles of methane per cc in the pore water [28-30]. Following dissociation, at 9.09 MPa and 13.4°C, $M_{FW} = 1.17 \times 10^{-4}$ moles of methane per cc in the pore water [28-30].

From the volume of confining fluid surrounding the sample in the chamber, a ~ 0.62 cc increase in sample volume is observed during dissociation. This volume increase must be taken up by the gas phase, because water and sand grains are relatively incompressible. The largest uncertainty is in estimating the pore space increase during dissociation, conservatively leading to an overall pore-space hydrate saturation uncertainty estimate of $\pm 0.1\%$.

With the added pore gas volume, a 0.33% increase in the total pore space, equation 2c becomes $V_G = 0.195 \cdot V_H + 0.0033$. The hydrate saturation V_H is $0.8 \pm 0.1\%$ of the total porosity. Over the entire 189 cc of pore space, an estimated 1.5 ± 0.2 cc of hydrate was formed.

4.2. Hydrate effect on permeability:

Given the circulating pump's flow rate and pressure measurements made in the inlet and outlet lines of the growth chamber, the sample permeability can be calculated using Darcy's law:

$$Q = \frac{kA}{\mu} \cdot \frac{\Delta P}{L}, \quad (3)$$

where the flow rate, Q , is given by the permeability, k , cross-sectional area of the sample, A , dynamic viscosity of the fluid, μ , and the pressure difference ΔP , driving flow through the sample of length L . Only the permeability relative to the initial permeability, k_0 , is of interest here, so assuming a constant cross-sectional area, sample length, and viscosity, the fractional permeability change is calculated as follows:

$$\frac{k}{k_0} = \frac{Q}{Q_0} \cdot \frac{\Delta P_0}{\Delta P}, \quad (4)$$

where Q_0 and ΔP_0 are the initial flow rate and pressure drop across the sample, respectively.

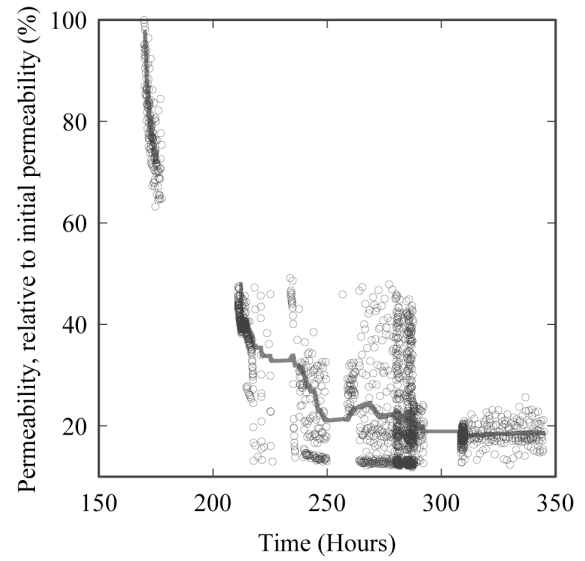


Figure 4: Permeability change in the sample during the continuous flow test (circles), and the 25-point running average (solid curve). Permeability drops by approximately a factor of 5 over the course of the hydrate formation process.

Hydrate formation causes the permeability to fall to approximately 20% of its original value (Fig. 4). Assuming hydrate forms only in the water-saturated sand and not in the sample endcaps, we can use the Kozeny-Carman formulation to constrain the hydrate distribution [31]:

$$\frac{k}{k_0} = \left(\frac{\phi}{\phi_0} \right)^3 \cdot \left(\frac{1-\phi_0}{1-\phi} \right)^2, \quad (5)$$

where ϕ_0 is 0.335, the initial hydrate-free sand porosity, and ϕ is the porosity of a homogeneous distribution of sand and hydrate. Given the calculated hydrate content of 1.5 ± 0.2 cc and the 72-mm sample diameter, Eq. 5 suggests the observed permeability decrease is due to $\sim 38\%$ pore space hydrate saturation in a ~ 2.7 mm layer of the otherwise water-saturated sand sample.

This distribution indicates the methane supersaturation may be too high upon entering the water-saturated sand, causing hydrate to form just as the methane-rich water enters the sample, choking off subsequent flow before hydrate can form more broadly within the sample. To allow methane-rich water to permeate the sample prior to hydrate formation, an episodic flow technique was employed in a subsequent test as described below.

4.3. Episodic flow technique:

To avoid the plugging problem encountered in the continuous-flow test, this technique is intended to uniformly distribute methane-rich water and hydrate particles obtained from the source chamber throughout the sand pack prior to cooling the sample in the absence of flow. In the presence of hydrate, cooling increases the water's methane supersaturation (Fig. 2), triggering additional hydrate growth nucleated around the hydrate particles.

Rewarming the sample reverses the process, increasing the pore-water methane solubility, and leading to hydrate dissolution. It is hoped that subsequent warming of the sample to 10°C and restarting flow of methane-rich water to replenish the methane concentration in the growth chamber can be accomplished quickly enough to avoid completely dissolving hydrate formed during the cooling cycle. Permeability measurements during periods of flow show no sign of a net increase in hydrate content from one cooling cycle to the next, however.

4.4. Verifying the absence of free gas:

Methane bubbles in an otherwise water-saturated sediment attenuate and slow compressional waves [32]. Figure 5 displays compressional wave measurements taken following hydrate formation in the continuous flow test (solid curve), compared to measurements taken in a water-saturated sand under identical pressure conditions (dashed curve). The hydrate-free sample has slightly less porosity than the hydrate-bearing sample initially contained, and correspondingly, has a slightly faster and stronger signal. Though the amplitude decrease is suggestive of methane gas, comparable wave speeds indicate the potential quantity of gas-phase methane is low.

4.5. Future direction:

To balance the rapid-formation objective with the tendency for rapid hydrate formation near the flow inlet to the growth chamber, ongoing tests will utilize a slow temperature-cooling ramp for the growth chamber. As with the tests presented here, more than ten total pore-volumes of methane- and hydrate-particle-rich water will pass through the growth chamber while the chamber is only slightly cooler than the source. Once the growth chamber is primed, flow will continue while the growth chamber is cooled slowly, starting from the downstream end of the sample, opposite the flow inlet.

By increasing the driving force for hydrate formation slowly, it is hoped methane and hydrate particles will initiate significant hydrate growth only after permeating the sample and moving away from the flow inlet.

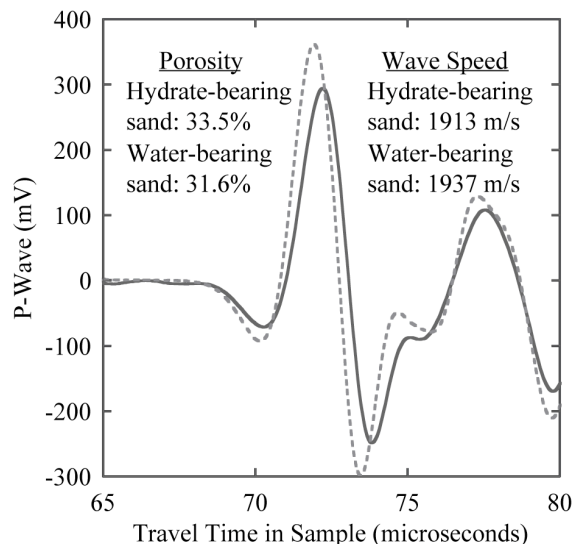


Figure 5: Compressional waveform in a hydrate-bearing sample (solid curve) closely matches the waveform through a water-saturated sand in which no hydrate or methane is present (dashed curve). Effective stress is the same for both samples. The similarity between wave speeds indicates free methane gas, which slows compressional waves, is not present in significant quantities.

5. CONCLUSIONS

Forming methane hydrate from dissolved-phase methane is critical for mimicking oceanic hydrate formation in marine sediments. To provide both the methane supersaturation and nucleation sites required for hydrate formation, a flow loop has been designed in which circulating water dissolves granular methane hydrate in a source chamber, thereby developing a well-constrained methane saturation while entraining hydrate micro-crystals that can shorten the induction period for hydrate formation in the growth chamber. This technique rapidly forms hydrate close to the flow inlet side of the sample, choking off subsequent flow. A temperature ramp approach for slowly building the hydrate formation driving force is under investigation.

6. ACKNOWLEDGMENTS

U.S. Geological Survey contributions were supported by the Gas Hydrate Project of the U.S. Geological Survey's Coastal and Marine Geology Program. USGS and Marine Desalinization Systems (MDS) contributions were also supported by Department of Energy Contract No. DE-AI21-92MC29214. Any use of trade names is for descriptive purposes only and does not imply endorsement by the U.S. Government.

REFERENCES

- [1] Kvenvolden, K.A., Natural gas hydrate; introduction and history of discovery, in *Natural Gas Hydrate In Oceanic and Permafrost Environments*, M.D. Max, Editor. 2000, Kluwer Academic Publishers: Dordrecht, Netherlands. p. 9-16.
- [2] Winters, W.J., W.P. Dillon, I.A. Pecher, and D.H. Mason, GHASTLI; determining physical properties of sediment containing natural and laboratory-formed gas hydrate, in *Natural Gas Hydrate In Oceanic and Permafrost Environments*, M.D. Max, Editor. 2000, Kluwer Academic Publishers: Dordrecht, Netherlands. p. 311-322.
- [3] Hornbach, M.J., W.S. Holbrook, A.R. Gorman, K.L. Hackwith, D. Lizarralde, and I. Pecher, Direct seismic detection of methane hydrate on the Blake Ridge. *Geophysics*, 2003. 68(1): p. 92-100.
- [4] Waite, W.F., W.J. Winters, and D.H. Mason, Methane hydrate formation in partially water-saturated Ottawa sand. *American Mineralogist*, 2004. 89: p. 1202-1207.
- [5] Priest, J.A., A. Best, and C.R. Clayton, A laboratory investigation into the seismic velocities of methane gas hydrate-bearing sand. *Journal of Geophysical Research*, 2005. 110: p. B04102, doi:10.1029/2004JB003259.
- [6] Tohidi, B., R. Anderson, M.B. Clennell, R.W. Burgass, and A.B. Biderkab, Visual observation of gas-hydrate formation and dissociation in synthetic porous media by means of glass micromodels. *Geology*, 2001. 29(9): p. 867-870.
- [7] Dvorkin, J., M.B. Helgerud, W.F. Waite, S.H. Kirby, and A. Nur, Introduction to physical properties and elasticity models, in *Natural Gas Hydrate In Oceanic and Permafrost Environments*, M.D. Max, Editor. 2000, Kluwer Academic Publishers: Dordrecht, Netherlands. p. 245-260.
- [8] Yun, T.S., F.M. Francisca, J.C. Santamarina, and C. Ruppel, Compressional and shear wave velocities in uncemented sediment containing gas hydrate. *Geophysical Research Letters*, 2005. 32: p. L10609, doi:10.1029/2005GL022607.
- [9] Buffett, B. and O. Zatsepina, Formation of gas hydrate from dissolved gas in natural porous media. *Marine Geology*, 2000. 164: p. 69-77.
- [10] Spangenberg, E., J. Kulenkampff, R. Naumann, and J. Erzinger, Pore space hydrate formation in a glass bead sample from methane dissolved in water. *Geophysical Research Letters*, 2005. 32: p. L24301, doi:10.1029/2005GL024107.
- [11] Helgerud, M.B., J. Dvorkin, A. Nur, A. Sakai, and T. Collett, Elastic-wave velocity in marine sediments with gas hydrates: Effective medium modeling. *Geophysical Research Letters*, 1999. 26(13): p. 2021-2024.
- [12] Yun, T.S., J.C. Santamarina, and C. Ruppel, Mechanical properties of sand, silt, and clay containing tetrahydrofuran hydrate. *Journal of Geophysical Research*, 2007. 112: p. B04106, doi:10.1029/2006JB004484.
- [13] Osegovic, J.P., S.R. Tatro, and S.A. Holman, Physical chemical characteristics of natural gas hydrate, in *Economic Geology of Natural Gas Hydrate*, M.D. Max, A.H. Johnson, and W.P. Dillon, Editors. 2006, Springer: Dordrecht, Netherlands. p. 45-104.
- [14] Katsuki, D., R. Ohmura, T. Ebinuma, and H. Narita, Formation, growth and ageing of clathrate hydrate crystals in a porous medium. *Philosophical Magazine*, 2006. 86(12): p. 1753-1761.
- [15] Stern, L.A., S.H. Kirby, S. Circone, and W.B. Durham, Scanning electron microscopy investigations of laboratory-grown gas clathrate hydrates formed from melting ice, and comparison to natural hydrates. *American Mineralogist*, 2004. 89(8-9): p. 1162-1175.
- [16] Stern, L.A., S.H. Kirby, and W.B. Durham, Peculiarities of methane clathrate hydrate formation and solid-state deformation, including possible superheating of water ice. *Science*, 1996. 273(5283): p. 1843-1848.
- [17] Stern, L.A., S.H. Kirby, and W.B. Durham, Polycrystalline methane hydrate: Synthesis from superheated ice, and low-temperature mechanical properties. *Energy & Fuels*, 1998. 12(2): p. 201-211.

- [18] Lu, W., I.M. Chou, and R.C. Burruss, Determination of methane concentrations in water in equilibrium with sI methane hydrate in the absence of a vapor phase by in situ Raman spectroscopy. *Geochimica et Cosmochimica Acta*, 2008. 72: p. 412-422.
- [19] Rehder, G., S.H. Kirby, W.B. Durham, L.A. Stern, E.T. Peltzer, J. Pinkston, and P.G. Brewer, Dissolution rates of pure methane hydrate and carbon dioxide hydrate in undersaturated seawater at 1000-m depth. *Geochimica et Cosmochimica Acta*, 2004. 68(2): p. 285-292.
- [20] Jhaveri, J. and D.B. Robinson, Hydrates in the methane-nitrogen system. *The Canadian Journal of Chemical Engineering*, 1965. 43: p. 75-78.
- [21] deRoo, J.L., C.J. Peters, R.N. Lichtenthaler, and G.A.M. Diepen, The occurrence of methane hydrate in saturated and unsaturated solutions of sodium chloride and water In dependence of temperature and pressure. *AIChE Journal*, 1983. 29(4): p. 651-657.
- [22] Yang, S.O., S.H. Cho, H. Lee, and C.S. Lee, Measurement and prediction of phase equilibria for water plus methane in hydrate forming conditions. *Fluid Phase Equilibria*, 2001. 185(1-2): p. 53-63.
- [23] Shpakov, V.P., J.S. Tse, C.A. Tulk, B. Kvamme, and V.R. Belosludov, Elastic moduli calculation and instability in structure I methane clathrate hydrate. *Chemical Physics Letters*, 1998. 282(2): p. 107-114.
- [24] Weast, R.C., *CRC Handbook of Chemistry and Physics*. 68 ed. 1987, Boca Raton: CRC Press, Inc.
- [25] Circone, S., S.H. Kirby, and L.A. Stern, Direct measurement of methane hydrate composition along the hydrate equilibrium boundary. *J. Phys. Chem. B*, 2005. 109: p. 9468-9475.
- [26] Duan, Z., N. Moller, and J.H. Weare, An equation of state for the CH₄-CO₂-H₂O system: I. Pure systems from 0 to 1000 °C and 0 to 8000 bar. *Geochimica et Cosmochimica Acta*, 1992. 56: p. 2605-2617.
- [27] Duan, Z. Pure phase systems - Methane. 2006
www.geochem-model.org/models/ch4/calc.php.
- [28] Sun, R. and Z.H. Duan, Prediction of CH₄ and CO₂ hydrate phase equilibrium and cage occupancy from ab initio intermolecular potentials. *Geochimica et Cosmochimica Acta*, 2005. 69(18): p. 4411-4424.
- [29] Duan, Z.H. and S.D. Mao, A thermodynamic model for calculating methane solubility, density and gas phase composition of methane-bearing aqueous fluids from 273 to 523 K and from 1 to 2000 bar. *Geochimica et Cosmochimica Acta*, 2006. 70(13): p. 3369-3386.
- [30] Duan, Z. Methane clathrate hydrate - Liquid equilibrium calculations. 2006 www.geochem-model.org/models/h2o_ch4/index.htm.
- [31] Mavko, G., T. Mukerji, and J. Dvorkin, *The rock physics handbook: Tools for seismic analysis in porous media*. 1998, Cambridge: Cambridge University Press. 329.
- [32] Yun, T.S., G.A. Narsilio, J.C. Santamarina, and C. Ruppel, Instrumented pressure testing chamber for characterizing sediment cores recovered at in situ hydrostatic pressure. *Marine Geology*, 2006. 229: p. 285-293.